SUPPLEMENTAL INFORMATION Neuron, Volume 67

Spatio-Temporal Response Properties of Optic-Flow Processing Neurons

F. Weber, C.K. Machens, and A. Borst

Inventory of Supplemental Information

Figures (with Legends):

- Figure S1, related to Figure 3
- Figure S2, related to Figure 4
- Figure S3, related to Figure 5

Experimental Procedures:

- *Dynamic Receptive Field Estimation* Using Linear Regression, related to the subsection *Estimation of the Dynamic Receptive Field* in Experimental Procedures
- *Reichardt Detector Array Stimulation*, related to the subsection *Biophysical Model for Optic-Flow Processing Neurons* in Experimental Procedures
- *Estimation of the Biophysical Model*, related to the subsection *Biophysical Model for Optic-Flow Processing Neurons* in Experimental Procedures
- *Predictive Power for Model Evaluation*, related to the subsection *Model Evaluation* in Experimental Procedures

SUPPLEMENTAL FIGURES

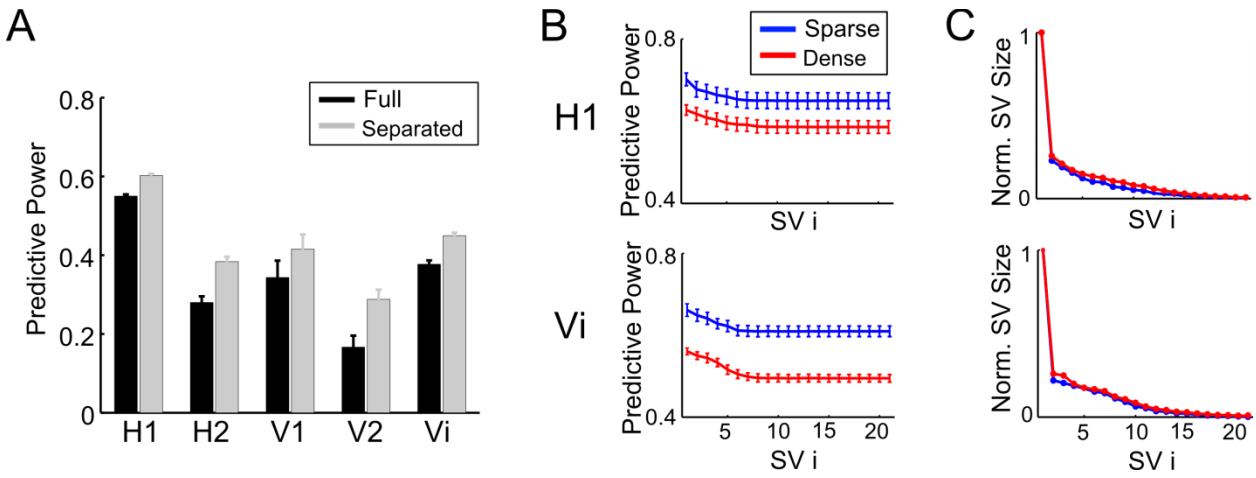

Figure S1 (related to Figure 3). Predictive Power for Dense Motion.

(A) For all recorded neurons, the predictive power of the space-time separated dynamic receptive field (Separated) is higher than for the full dynamic receptive field (Full). Error bars denote the S.E.M.

(B) Increasing the number of spatial and temporal components in the dynamic receptive field (DRF) reduces the model performance. The predictive power of the dynamic receptive field of an H1 (top) and Vi cell (bottom) are plotted as a function of the number of non-zero singular values. A singular value of 1 refers to the performance of the space-time separated model, a singular value of 21 corresponds to the full dynamic receptive field (error bars: S.E.M.). (The evaluation was done on the same recordings as presented in Figures 3C and 3D).

(C) Normalized size of the singular values obtained from singular value decomposition of the full dynamic receptive field (DRF). As expected from the space-time separability, the full DRF has only one large singular value.

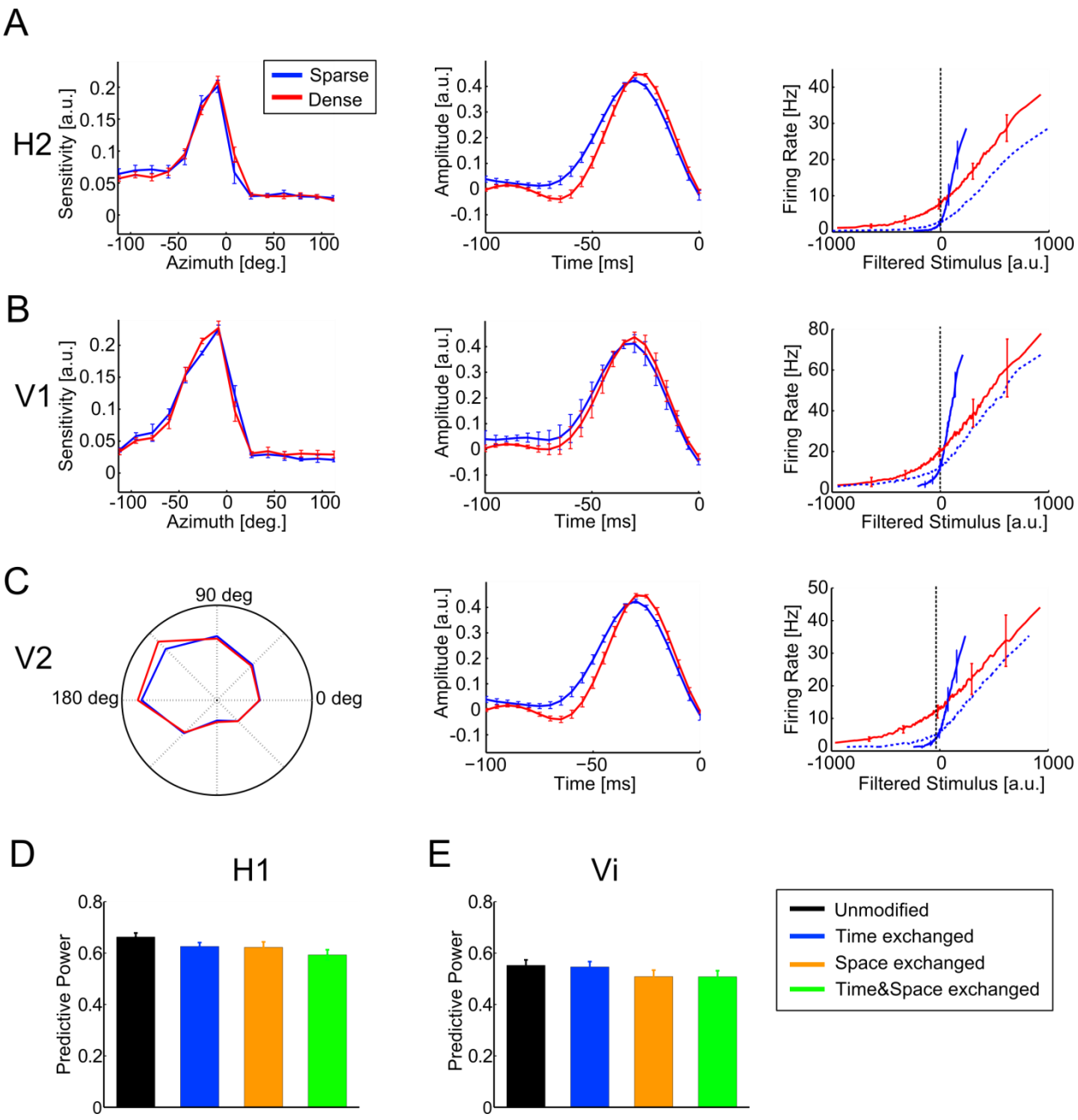

Figure S2 (related to Figure 4). Changes in the DRFs of H2, V1 and V2 due to an Increased Density of Motion Cues.

(A,B,C) Comparison of the spatial and temporal components and static nonlinearities of H2, V1 and V2. (Left) Sensitivity tuning curves for sparse (blue) and dense motion (red). The sensitivity tuning curves for H2 and V1 were computed as for H1 (see Figure 4A left). The curves for V2 were determined analogously to Vi (see Figure 4B left). (Middle) Averaged temporal components for sparse (blue) and dense motion (red). (Right) Static nonlinearities for sparse (Sparse, blue) and dense motion (Dense, red). An increase of

the number of motion cues results in a decrease of the gain and selectivity. Error bars represent the S.E.M.

(D, E) The DRF components estimated for dense motion perform also well for predicting the neural response to sparse motion. The performance of the space-time separated LN-model (Unmodified, black) of H1 (D) and Vi (E) is compared to three modified model versions: (1) The temporal component estimated for sparse motion was replaced by the temporal component estimated for dense motion (Time exchanged, blue). (2) The spatial component for sparse motion was replaced by the spatial component for dense motion (Space exchanged, orange). (3) Both the spatial and temporal component were replaced by the respective components for dense motion (Space&Time exchanged, green). Error bars denote the S.E.M. (The values for 'Unmodified' are the same as depicted in Figure 3B for the 'Separated' model of H1and Vi.)

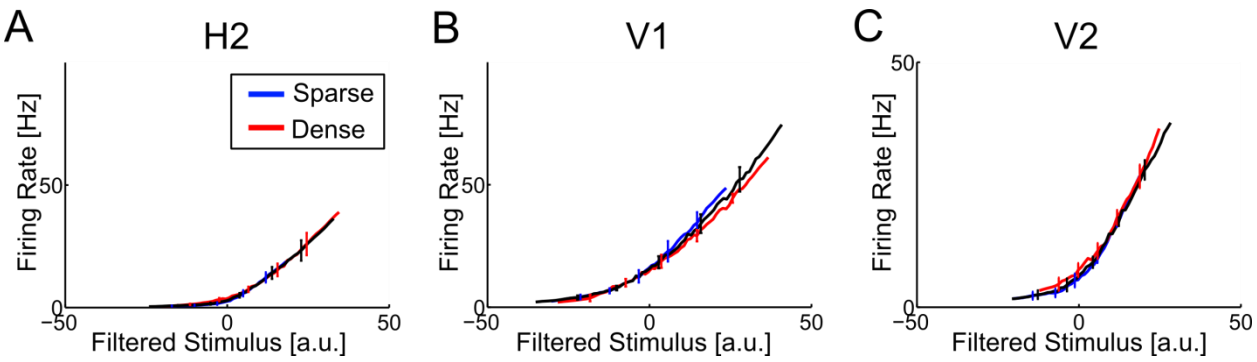

Figure S3 (related to Figure 5). Static Nonlinearities of the Biophysical Model for H2, V1, and Vi.

(A-C) For all three neurons, the nonlinearity estimated for both stimulus conditions (black) is shown together with the nonlinearities determined separately for sparse and dense motion (blue and red). The close overlap of the nonlinearities indicates that the biophysical model indeed compensates for the divisive and additive modulation of the input-output relation. Error bars represent the S.E.M.

SUPPLEMENTAL EXPERIMENTAL PROCEDURES

Notation

In the following we use the following notation: Vectors are written as small bold-face letters, matrices as large bold-face letters. If the vector $\mathbf{r}$ describes the discretized version of the time function $r(t)$, then the vector element at time point t_i is referenced as $r(t_i)$ or as r_i. Similarly, if $\mathbf{M}$ represents the discretized version of the two-dimensional function $M(\phi,\theta)$, the function value at grid location (ϕ_i,θ_j) is denoted as $M(\phi_i,\theta_j)$ or $M_{i,j}$.

Estimation of the Dynamic receptive field

The dynamic receptive field is specified by the linear kernels $H_{az}(\phi_i,\theta_j,t_k)$ and $H_{el}(\phi_i,\theta_j,t_k)$ (see Estimation of the Dynamic Receptive Field in Exp. Procedures). To find the optimal linear kernels which minimize Equation 2, we first formulated a constrained linear system of equations. For this purpose, we re-ordered indices such that $v_{lm} = V_{el}(\phi_i,\theta_j,t_{l-k+1})$ with $m = n_{el}n_{az}(k-1) + (j-1)n_{el} + i$ and $v_{ln} = V_{az}(\phi_i,\theta_j,t_{l-k+1})$ with $n = m + K\,n_{el}n_{az}$. Similarly, we set $h_m = H_{el}(\phi_i,\theta_j,t_k)$ and $h_n = H_{az}(\phi_i,\phi_j,t_k)$ (using the same definition for m and n). Without loss of generality, we centered the measured response and the stimulus such that $\sum_i r_i = 0$ and $\sum_i v_{ij} = 0$ for each column j. Then equation 4 can be rewritten as, $r_l = \sum_{j=1}^{N} v_{lj}\,h_j$ with $N = 2\,n_{el}n_{az}\,K$. The optimal parameters h_j are obtained by minimizing the mean square error between the estimated response, $\hat{r}_i$, and, the measured response, r_i,

$$Err = \frac{1}{2}\sum_{i=1}^{M}(r_i - \sum_{j=1}^{N} v_{ij}h_j)^2 + \frac{1}{2}\sum_{i=j}^{N}\lambda\,h_j^2, \qquad \text{(S1)}$$

where M refers to the number of recorded response bins. The second term forces the kernel elements h_j to be small and decreases the contribution of poorly sampled stimulus directions to the final estimate for h_i (Bishop, 2008). Setting the derivative of Err with respect to h_j to zero and rearranging gives the optimal solution. Introducing $a_k = \sum_{i=1}^{M} v_{ik}r_i$ and $B_{jk} = \sum_{i=1}^{M} v_{ij}v_{ik}$, the solution is given by

$$h_j = \sum_{k=1}^{N} (\mathbf{B} + \lambda)^{-1}_{jk} \; a_k, \qquad \text{(S2)}$$

where the negative exponent denotes the matrix inverse. (Bold face letters refer to vectors or matrices.)

Reichardt Detector Array Simulation

For the biophysical model, we simulated the conductances of synapses connecting the local elementary motion detectors to the tangential cells (see Biophysical Model for Optic-Flow Processing Neurons in Exp. Procedures). The response properties of the fly tangential cells can be well described by assuming that they integrate the synaptic outputs of Reichardt detectors (Borst et al., 1995; Lindemann et al., 2005). We simulated the responses of the pre-synaptic elementary motion detectors to the Brownian motion stimuli using an array of Reichardt-detectors with a sampling base of 2.5 deg. In the Reichardt model, the luminance signals at two horizontally or vertically neighboring locations are correlated to compute a motion prediction. For a horizontally tuned motion detector, the luminance signals $S_{az}(\phi_i, \theta_j)$ and $S_{az}(\phi_{i+1}, \theta_j)$, at locations (ϕ_i, θ_j) and (ϕ_{i+1}, θ_j), were fed through a low-pass and high-pass filter and subsequently multiplied,

$$G_{az}^{exc}(\phi_i, \theta_j, t) = \left(S_{az}(\phi_i, \theta_j, t) * LP(t)\right) \left(S_{az}(\phi_{i+1}, \theta_j, t) * HP(t)\right) \qquad \text{(S3)}$$

with '*' denoting the convolution operator. $LP(t)$ denotes a first-order low-pass filter with time constant τ_{LP}. The time constant of the first-order high-pass filter $HP(t)$ is denoted by τ_{HP}. A second multiplication is performed in a mirror symmetrical way,

$$G_{az}^{inh}(\phi_i, \theta_j, t) = \left(S_{az}(\phi_i, \theta_j, t) * HP(t)\right) \left(S_{az}(\phi_{i+1}, \theta_j, t) * LP(t)\right) \qquad \text{(S4)}$$

The subtraction

$$V_{az}(\phi_i, \theta_j, t) = G_{az}^{exc}(\phi_i, \theta_j, t) - G_{az}^{inh}(\phi_i, \theta_j, t) \qquad \text{(S5)}$$

then yields an estimate for horizontal motion at location $(\phi_{i,}\theta_j)$. Biophysically, the subtraction in Equation 9 is implemented via an excitatory and inhibitory synapse, both projecting onto the tangential cell's dendrite. The corresponding synaptic conductances are given by $G_{az}^{exc}(\phi_i, \theta_j, t)$ and $G_{az}^{inh}(\phi_i, \theta_j, t)$. To ensure that all synaptic conductances are positive, negative values for $G_{az}^{exc}(\phi_i, \theta_j, t)$ were interpreted as (positive) inhibitory conductances and vice versa.

The vertical motion prediction $V_{el}(\phi_i, \theta_j, t)$ was computed analogously by correlating the luminance signals $S_{el}(\phi_i, \theta_j, t)$ and $S_{el}(\phi_i, \theta_{j+1}, t)$.

Note that the presented stimuli where fed through a Reichardt detector array consisting of rightward and upward tuned Reichardt detectors. If, however, for a particular neuron, the detector at position (ϕ_i, θ_j) is leftwards or downwards tuned, $G_s^{inh}(\phi_i, \theta_j, t_k)$ has to be substituted by $G_s^{exc}(\phi_i, \theta_j, t_k)$ and vice versa.

Estimation of the Biophysical Model

The biophysical model is completely described by the synaptic weight matrices $W_{az}(\phi_i, \theta_j)$ and $W_{el}(\phi_i, \theta_j)$, the temporal filter $b(t_k)$, the dendritic integration parameters A, c, D, z and the current-discharge curve f (see Equation 5 in Exp. Procedures). All parameters were directly derived from the recorded data through minimization of an error function.

For the LN-model, the spatial and temporal component were obtained from singular decomposition of the (re-arranged) full dynamic receptive field (DRF) and can be seen as the most significant dimensions of the DRF. Analogously $W_s(\phi_i, \theta_j)$ and $b(t_k)$ can be interpreted as the most significant dimensions of the higher order-rank matrices $P_s(\phi_i, \theta_j)$ with $s \in \{az, el\}$ specifying a DRF. $P_s(\phi_i, \theta_j)$ can then be approximated by a rank-one matrix given by the product of the synaptic weight matrix $W_s(\phi_i, \theta_j)$ and the temporal filter $b(t_k)$, i.e. $P_s(\phi_i, \theta_j, t_k) = W_s(\phi_i, \theta_j) b(t_k)$.

To optimize I_{siz}, we minimized the error function given by

$$Err(A, c, D, z, \mathbf{P_{az}}, \mathbf{P_{el}}) = \frac{1}{2}\sum_{i=1}^{N}\left(r_i - I_{siz}(t_i)\right)^2, \qquad \text{(S6)}$$

where r_i again refers to the firing rate at t_i. This error function was optimized using conjugate gradient descent. To minimize *Err,* we preceded as follows: In a first run of the applied algorithm, we optimized for A, c and $\mathbf{P}_s$ without constraints on the rank and length of $\mathbf{P}_s$. From the obtained matrices $\mathbf{P}_s$, we then extracted an estimate for $\mathbf{W_s}$ and $\mathbf{b}$ through singular value decomposition of $\mathbf{P}_s$. The values for $\mathbf{W}_s$ and $\mathbf{b}$ were then used as start vectors for a second optimization where $\mathbf{W}_s$ and $\mathbf{b}$ were refined. Given the resulting estimates for $\mathbf{W}_s$ and $\mathbf{b}$, we then re-optimized in two further runs *A* and c and finally D and z. In the end, we estimated *f* by comparing the prediction given by I_{siz} with the recorded firing rate as described above (see Estimation of Static Nonlinearities in Exp. Procedures**)**.

Predictive Power for Model Evaluation

The ability of a given model to predict the correct firing rate in response to a given stimulus can be measured by the mean square error between estimated and measured response, $\sigma_e^2 = \langle \frac{1}{M} \sum_i (r_i - \hat{r}_i)^2 \rangle$ (the angular brackets denote trial averaging). However, since the response normally includes non-stimulus related noise, the error of an even perfect fit will be larger than zero. To account for the noise in the recorded signal, (Sahani & Linden, 2003) proposed an alternative measure to evaluate the model performance: Assuming that the recorded response is additively composed of a stimulus-related signal and non-stimulus related noise, the lowest value σ_e^2 can reach is the residual noise component. The latter can be estimated by

$$\sigma_\eta^2 = \frac{n}{n-1} \left[\langle \frac{1}{M} \sum_i r_i^2 \rangle - \frac{1}{M} \sum_i \langle r_i \rangle^2 \right], \qquad \text{(S7)}$$

where n is the number of trials. Given the response power $\sigma_r^2 = \langle \frac{1}{M} \sum_i r_i^2 \rangle$, the relative success of the model is given by

$$\beta = \frac{\sigma_r^2 - \sigma_e^2}{\sigma_r^2 - \sigma_\eta^2}, \qquad \text{(S8)}$$

which is 1 when the mean square error σ_e^2 equals the signal noise. Generally, β can be interpreted as the percentage of the stimulus-related response power, $(\sigma_r^2 - \sigma_\eta^2)$, that

can be explained by the given model. We calculated the predictive power of a given model on the training and on the test sets as obtained from a 5-fold cross-validation. The relative success on the training sets, β_{train}, gives an upper bound for the predictive power of a model. The relative success on the unknown test sets, β_{test}, sets a lower bound for the quality of the model under question. The constraint parameter λ for the estimation of the dynamic receptive fields (see Equation S1) was chosen such that it maximizes the lower bound of the predictive power, β_{test}. In this study, we always used the lower bound, β_{test}, to quantify the predictive power of a model.